Dissipative-particle-dynamics model for two-phase flows

Anupam Tiwari* and John Abraham†
School of Mechanical Engineering, Purdue University, West Lafayette, Indiana 47907, USA
(Received 4 May 2006; revised manuscript received 8 September 2006; published 1 November 2006)

Dissipative particle dynamics (DPD) is a mesoscopic method in which coarse graining is done at the molecular level to capture the physics at the meso level. In this paper, we present a DPD model for two-phase flows involving liquid and vapor phases. The model is based on mean-field theory. Phase segregation between the two phases is simulated by the choice of an equation of state with a van der Waals loop. Surface tension is modeled by a term that depends on higher-order density gradients and accounts for long-range attractive forces. To test the model, we present results from simulations of a liquid layer, several liquid cylinders of varying size to verify the Laplace's law, small- and large-amplitude liquid cylinder oscillations and capillary waves. In all these cases we compare DPD results with results available from analytical solutions.

DOI: 10.1103/PhysRevE.74.056701 PACS number(s): 47.11.−j, 02.70.Ns, 47.55.Kf, 04.60.Nc

I. INTRODUCTION

Two-phase flows in which interfacial physics is important arise in several applications. These include liquid jet breakup, drop collisions, and drop breakup. Experimental studies of such flows by themselves are not able to provide a complete understanding of the physics because of the multiple scales associated with the physical situation, not all of which can be resolved. Computational methods hold out the possibility of having fully controlled "numerical" experiments to investigate the influence of physical parameters. Due to the complex underlying physics of the problems, however, computational investigations are also challenging as the simulation of the interface requires information about its location and shape, which needs to be determined along with the flow field. Conventional approaches to these problems include front-tracking [1] and front-capturing methods [2,3] that involve solution of the Navier-Stokes equations. More recently lattice-Boltzmann methods (LBM) [4–6] have been employed for these simulations [7,8].

When the length scales of interest in a problem lie between the molecular and macroscopic levels, then mesoscopic simulations, in which coarse graining is done to obtain the relevant length and time scales, are promising. The term mesoscopic means a degree of spatial and temporal resolution where we can capture phenomena that occur within length scales of 10–1000 nm and time scales of 1 ns–10 ms [9]. An advantage of using mesoscopic methods for modeling two-phase systems is that the interfacial forces can be incorporated from a fundamental viewpoint starting from an equation of state. An interface can be maintained between the two phases without an explicit need for tracking or capturing it.

Dissipative particle dynamics (DPD) [10] is a relatively new particle-based mesoscopic method that includes thermal fluctuations and offers flexibility in choosing an interparticle potential. In DPD, a coarse graining is done at the molecular level to capture the physics at the meso level. Hence, each DPD particle represents a cluster of actual molecules that interact according to certain rules. DPD has been applied to various complex systems such as polymer suspensions [11–17], colloids [18–20], drops in shear field (using a binary fluid model) [21,22], and flow of biological matter [23].

The binary fluid model of DPD has been used for simulations of domain growth and phase separation by Coveney *et al.* [24]. Dzwinel *et al.* [25] used the binary fluid model to simulate Rayleigh-Taylor instability in the mesoscale. Although some progress has been made [26–29], the modeling of two-phase flows with DPD remains largely unexplored. Three models have been proposed in the literature for two-phase systems involving a liquid and vapor phase. Pagonabarraga *et al.* [26,27] developed a model in which they introduced a density-dependent term for the conservative force. They used a modified van der Waals equation of state, which had additional contributions from terms cubic in density. They used the same cut-off radius for the attractive and repulsive components of the conservative force between the DPD particles. In their model, as pointed out by the authors, the sign of surface tension is dependent on the choice of simulation parameters for the equation of state. A model proposed by Warren [28,30] employed a form of conservative force that had different cut-off radii for the attractive and repulsive components of forces of interaction. This model was developed for the simulation of free-surface flows. Liu *et al.* [29] suggested a model based on different influence ranges for attractive and repulsive forces. This is similar in concept to the model proposed by Warren [28,30].

In this work, we have developed a model in which the free energy of the fluid has a dependence on density and its gradients. These gradients account for the excess free energy in the interfacial region and are related to the long-range attractive forces. This gives a diffuse-interface [31] formulation for DPD in which the density varies smoothly between the liquid and vapor phases. The conservative force is modeled as a central force whose amplitude depends on density and its gradients. The terms dependent on density gradients become important in the interfacial region and give rise to surface tension. The strength of surface tension can be controlled using a free parameter. We have tested the model for static simulations of a liquid layer and verification of Laplace's law. The model has also been tested for problems

*Electronic address: tiwari0@ecn.purdue.edu
†Electronic address: jabraham@ecn.purdue.edu

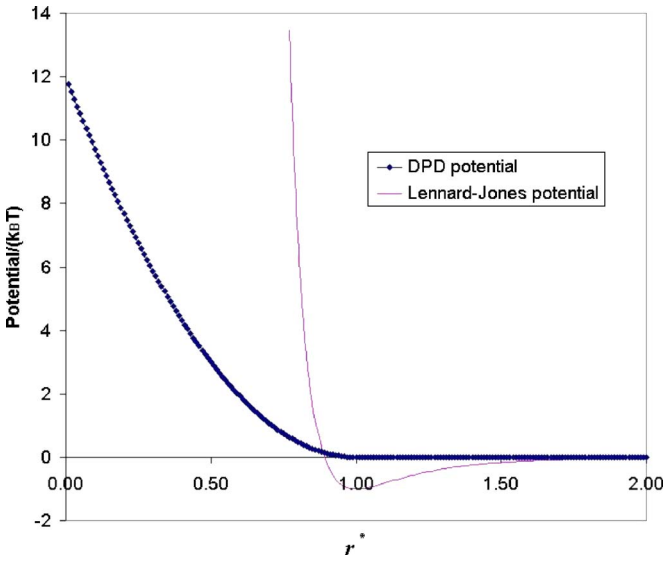

FIG. 1. (Color online) Hard-core Lennard-Jones potential vs the soft-core DPD potential; $r^*=r/\sigma_0$ for the Lennard-Jones potential, $r^*=r/r_c$ for DPD, see text.

involving interfacial dynamics. These include the small- and large-amplitude oscillations of liquid cylinders and simulations of capillary waves. Development of DPD two-phase models is of interest as DPD has the potential to simulate problems where thermal fluctuations control the outcome. For example, the model developed here can be used for studying thermally induced breakup of liquid cylinders as done by Kawano [32] using molecular dynamics. It can also be used for studying the breakup of nanojets where the continuum theory over predicts the breakup length as shown by the molecular dynamics simulations of Moseler *et al.* [33].

This paper is organized as follows. In Sec. II, we describe the two-phase DPD model. In Sec. III, we will present results from the numerical simulations of a liquid layer problem, verification of Laplace's law, small- and large-amplitude oscillations of liquid cylinders, and capillary waves. We will also present the results from liquid cylinder formation in liquid-vapor simulations performed at different temperatures. We will conclude the paper in Sec. IV with summary and conclusions.

II. THE TWO-PHASE DPD MODEL

In this section, a description of the two-phase DPD model will be provided. As stated earlier, DPD is a coarse grained representation of molecular dynamics (MD) [34–36]. A popular model for the interatomic potential in MD simulations is the Lennard-Jones 6-12 potential, graphically represented in Fig. 1. In this figure, r^* on the x coordinate is r/σ_0 for the Lennard-Jones potential where r is the interatomic separation and σ_0 is the atomic diameter. We see from this figure that the Lennard-Jones potential has a steep slope for lower values of interatomic separation that restricts the numerical time step that can be taken. This steep slope gives a *hard-core* nature to the Lennard-Jones potential. A characteristic length for the Lennard-Jones potential is the atomic diameter, which is of the order of a few Angstroms. If we are interested in meso-level simulations, MD might prove to be unjustifiably expensive from a computational point of view. In this case, we can do a coarse graining at the molecular level by packing actual atoms/molecules together to form virtual particles. This is the essence of dissipative particle dynamics (DPD). The virtual particles are the DPD particles. The coarse graining results in the *softening* of the hard-core interatomic potential as shown in Fig. 1. In this figure, for the DPD potential r^* is r/r_c where r is the interparticle separation and r_c is the cut-off radius [see Eq. (2)]. The *soft-core* DPD potential has a slope that is much shallower than the slope of the hard-core Lennard-Jones potential. Due to this, we can take time steps in DPD that are much larger than those possible in MD computations. The characteristic length for this potential is in the meso level, which is several orders of magnitude greater than the length scale for the Lennard-Jones potential. The description of the model below includes a brief discussion of the DPD method followed by a detailed discussion of the two-phase model. We use an isothermal DPD model in this work. For performing simulations at a constant total energy of the system, energy conserving forms of DPD have also been proposed in literature [37,38].

Dissipative particle dynamics considers a system of N particles in continuous space. The motion of any DPD particle i is governed by Newton's laws given by

$$\frac{d\mathbf{r}_i}{dt}=\mathbf{v}_i,$$

$$\frac{d\mathbf{v}_i}{dt}=\mathbf{f}_i, \tag{1}$$

where $\mathbf{r}_i$, $\mathbf{v}_i$, and $\mathbf{f}_i$ denote its position, velocity and the force that acts on it, respectively. In writing Eq. (1) the mass of the DPD particle has been taken to be unity.

The force of interaction between DPD particles is split into three components, namely the dissipative, random, and conservative forces. The dissipative force is responsible for the viscous effects in the system and it acts like a viscous damper by reducing the relative velocity between DPD particles. The random force is added to account for the lost degrees of freedom. This loss is incurred because of the coarse graining that is done at the molecular level to capture physics at the meso level. So we see that the dissipative force tends to *cool* down the DPD system while the random force tends to *heat* it up. So, for an isothermal system a balance condition is required between these components to maintain a constant temperature for the system. This is achieved by applying the fluctuation-dissipation theorem [39]. This balance condition will be shown later in this section. The dissipative and random forces are responsible for the *hydrodynamic* behavior of the system. The conservative force is responsible for the *thermodynamic* behavior of the DPD system. All the forces are short-range in nature and have a range equal to the cut-off length r_c of the model. The three forces, namely, dissipative, $\mathbf{F}_{ij}^D$, random, $\mathbf{F}_{ij}^R$, and conservative, $\mathbf{F}_{ij}^C$, between two DPD particles i and j are given by

$$\mathbf{F}_{ij}^{D} = -\gamma\omega^{D}(r_{ij})(\mathbf{e}_{ij}\cdot\mathbf{v}_{ij})\mathbf{e}_{ij},$$

$$\mathbf{F}_{ij}^{R} = \sigma\omega^{R}(r_{ij})\xi_{ij}\mathbf{e}_{ij}, \tag{2}$$

and

$$\mathbf{F}_{ij}^{C} = -\frac{\partial\psi(r_{ij})}{\partial r_{ij}}\mathbf{e}_{ij}.$$

Here, $\mathbf{e}_{ij}$ is a unit vector given by $\mathbf{e}_{ij}=\mathbf{r}_{ij}/|\mathbf{r}_{ij}|$, where $\mathbf{r}_{ij}=\mathbf{r}_i-\mathbf{r}_j$, $\mathbf{v}_{ij}=\mathbf{v}_i-\mathbf{v}_j$, γ is the amplitude of the dissipative force, σ is the amplitude of random force, ω^D and ω^R are the weight functions for the dissipative and random forces, respectively, and ψ is the free energy per particle. The term ξ_{ij} in Eq. (2) is a random variable that follows Gaussian statistics and has the following properties:

$$\langle\xi_{ij}(t)\rangle = 0,$$

$$\langle\xi_{ij}(t)\xi_{kl}(t')\rangle = (\delta_{ik}\delta_{jl}+\delta_{il}\delta_{jk})\delta(t-t'). \tag{3}$$

The form of conservative force which has been chosen by many researchers [40] for their single-phase and binary fluid simulations is a linear function in interparticle separation having a fixed maximum value that it can attain. This form of conservative force $\mathbf{F}_{ij}^{C}$ between particles i and j is given by

$$\mathbf{F}_{ij}^{C} = a_{ij}\left(1-\frac{r_{ij}}{r_c}\right)\mathbf{e}_{ij}, \tag{4}$$

where a_{ij} is a repulsion parameter between particles i and j. It is the maximum value of the conservative force and is related to the compressibility of the fluid being modeled [40,41], r_{ij} is the interparticle separation, r_c is the cut-off radius, and $\mathbf{e}_{ij}$ is the unit vector from particle j to i. From Eq. (2) we see that the conservative force is derived from the free energy. So, we can model a variety of physical systems given a form of free energy. In fact, we can also use the Lennard-Jones potential to derive the conservative force in DPD. For this case, the dissipative and random forces would act as a thermostat for the molecular dynamics system. Soddemann *et al.* [42] have shown that DPD is a useful thermostat for molecular dynamics systems when the interest lies in studying the hydrodynamic behavior of the system. They showed that the DPD thermostat allows for larger time steps as compared to the time steps possible for constant energy simulations in MD.

The manner in which the pair-wise forces are defined along with the use of relative positions and velocities makes the DPD method fully isotropic and Galilean invariant. It is possible to derive the macroscopic conservation equations starting from the DPD equations of motion given in Eq. (2). This derivation, along with the calculation of transport properties of a DPD fluid based on simulation parameters, has been presented in the literature by several authors [43–46].

Espanol *et al.* [47] showed that DPD recovers the correct Gibbs-Boltzmann distribution at equilibrium if the coefficients and the weight functions in the dissipative and random forces are related by

$$\omega^{D}(r) = [\omega^{R}(r)]^2, \quad \sigma^2 = 2\gamma k_B T. \tag{5}$$

Equation (5) is a balance condition between the dissipative and random forces for an isothermal DPD system and is derived by applying the fluctuation-dissipation theorem [39].

Groot *et al.* [40] have shown through a heuristic argument that the random force takes the form

$$\mathbf{F}_{ij}^{R} = \sigma\omega^{R}(r_{ij})\theta_{ij}(\delta t)^{-1/2}\mathbf{e}_{ij}, \tag{6}$$

where θ_{ij} is a random number that follows Gaussian statistics and has zero mean and unit variance. The weight functions for the dissipative and the random forces are taken to be

$$\omega^{D}(r) = [\omega^{R}(r)]^2 = \begin{cases} \left(1-\dfrac{r}{r_c}\right)^2, & (r<r_c) \\ 0, & (r\geqslant r_c). \end{cases} \tag{7}$$

Details about the choice of simulation parameters in DPD are given in the article by Groot *et al.* [40]. In this work, the equations of motion have been integrated using the modified-Verlet scheme of Groot *et al.* [40]. This scheme is given by

$$\mathbf{r}_i(t+\delta t) = \mathbf{r}_i(t) + \delta t\mathbf{v}_i(t) + \frac{1}{2}(\delta t)^2\mathbf{f}_i(t),$$

$$\tilde{\mathbf{v}}_i(t+\delta t) = \mathbf{v}_i(t) + \lambda\delta t\mathbf{f}_i(t),$$

$$\mathbf{f}_i(t+\delta t) = \mathbf{f}_i(\mathbf{r}(t+\delta t),\tilde{\mathbf{v}}(t+\delta t)),$$

$$\mathbf{v}_i(t+\delta t) = \mathbf{v}_i(t) + \frac{1}{2}\delta t[\mathbf{f}_i(t)+\mathbf{f}_i(t+\delta t)], \tag{8}$$

where $\mathbf{r}$, $\mathbf{v}$, and $\mathbf{f}$ denote the position, velocity, and force vectors, respectively, t denotes time, i denotes a particle tag, and λ denotes an empirical parameter. In this algorithm, a guessed value $\tilde{\mathbf{v}}$ for velocity is used for calculating the forces, which are velocity dependent as seen in Eq. (2). This guess is later corrected in the last step of the algorithm.

Now, we will turn our attention to the two-phase model, the development of which is the primary contribution of this work. As discussed earlier, the dissipative and random forces are responsible for the hydrodynamic while the conservative force is responsible for the thermodynamic behavior of the system. The modeling of two-phase systems is dependent on the thermodynamic behavior of the system. Hence, we turn our attention to the conservative force. The form of conservative force shown in Eq. (4) gives an equation of state that is quadratic in density [40] and a potential as shown in Fig. 1. To model a two-phase system involving liquid and vapor phases, we need an equation of state with a van der Waals loop as shown in Fig. 2. The part of the equation of state that lies between points b and c in this figure has negative compressibility which is unphysical. Hence, we cannot have a stable two-phase system in this part of the p-v diagram. This constraint leads to a segregation of the liquid and vapor phases, the density of which is determined by Maxwell's equal area points a and d [48]. An examination of Fig. 1 reveals that the DPD potential corresponding to the conservative force in Eq. (4) does not carry information about the

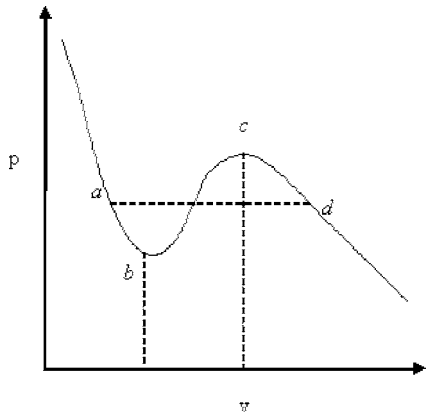

FIG. 2. P-v diagram for a van der Waals equation of state.

long-range attractive forces which are responsible for surface tension between the liquid and vapor phases. To account for these long-range attractive forces, we turn to mean-field theory [49,50], which provides a methodology for compensating this lost information. The mean-field value of free-energy per particle is given by [50]

$$\psi_m = \int u_{att}(r)\rho d\mathbf{r}, \tag{9}$$

where u_{att} is the attractive part of interaction potential, r is the interparticle separation, and ρ is the number density. Using a Taylor series expansion for density only the even derivatives of density survive and we get the following expression for free energy:

$$\psi_m = -a\rho - \kappa\nabla^2\rho, \tag{10}$$

where

$$a = -\frac{1}{2}\int_{r>\sigma_0} u_{att}(r)d\mathbf{r},$$

and

$$\kappa = -\frac{1}{6}\int_{r>\sigma_0} r^2 u_{att}(r)d\mathbf{r}, \tag{11}$$

in which σ_0 is the molecular diameter. The parameters a and κ arise due to the long-range attractive forces and give rise to the weak attraction and surface tension, respectively, between the DPD particles at the coarse-grained level.

Now we are in a position to formulate the conservative force. The form of the conservative force $\mathbf{F}^C$, which gives rise to phase segregation and surface tension in a liquid-vapor system, is given by

$$\mathbf{F}^C = -\nabla\psi_{nonideal} + \mathbf{F}^S, \tag{12}$$

where $\psi_{nonideal}$ represents the nonideal part of the free energy ψ and superscript S represents the surface tension component. The first term in the equation above represents the contribution due to the nonideal part of the equation of state. We consider the contribution only from the nonideal part because the ideal part has already been considered through the random and dissipative components.

In this work, we use the van der Waals equation of state given by

$$p = \frac{\rho k_B T}{1 - b\rho} - a\rho^2, \tag{13}$$

where a and b are the parameters for the equation of state, k_B is the Boltzmann constant, T is the temperature, and ρ is the number density. As seen in Eq. (11) the parameter a accounts for the long-range attractive behavior. The parameter b is responsible for exclusion volume effects. The free energy can be derived from Eq. (13) by using the relation

$$p = -\frac{\partial\psi}{\partial v}, \tag{14}$$

where p is the pressure and v the specific volume. Using the expression for equation of state in Eq. (13), the expression for free energy ψ is

$$\psi = -k_B T \ln(1 - b\rho) - a\rho + k_B T \ln\rho. \tag{15}$$

The first term arises due to the exclusion volume effects and is responsible for repulsion between the particles. The origin of the second term in this equation is seen in Eq. (10). The third term arises from the ideal part of the equation of state. In Eq. (12) we need only the nonideal part which is obtained by subtracting the ideal component from Eq. (15) and is given by

$$\psi_{non\text{-}ideal} = -k_B T \ln(1 - b\rho) - a\rho. \tag{16}$$

We see that the nonideal part of free energy is dependent on the density of particles. Hence, we need a methodology for density calculation. We calculate the density in the vicinity of a particle i as a weighted average of contributions from its neighbors within its interaction range. This definition is also used for density calculations in smoothed particle hydrodynamics [51] and is given by

$$\rho_i = \sum_{j=1}^{N} w(r_{ij}), \tag{17}$$

where i and j are particle tags, N is the number of particles, r_{ij} is the interparticle separation, and w is the normalized weight function such that $\int_0^{r_c} 2\pi r w(r)dr = 1$ for two-dimensional systems. For reasons that will be discussed later, we choose the Lucy weight function [52] for density calculations, which is different from the weight functions used in the calculation of dissipative and random forces in Eq. (7). This weight function w for a two-dimensional case is given by

$$w(r, r_c) = \begin{cases} \dfrac{5}{\pi r_c^2}\left(1 + \dfrac{3r}{r_c}\right)\left(1 - \dfrac{r}{r_c}\right)^3 & \text{if } r < r_c \\ 0 & \text{if } r > r_c, \end{cases} \tag{18}$$

where r is the interparticle separation and r_c is the cut-off radius for the DPD method.

When the mean-field theory is employed, the form taken by the surface tension force $\mathbf{F}^S$ in Eq. (12) is given by

$$\mathbf{F}^S = \kappa \nabla \nabla^2 \rho, \tag{19}$$

where κ is the surface tension parameter appearing in Eq. (11) and ρ is the number density. This form is evident from the expression for mean-field free energy in Eq. (10). Substituting Eqs. (16) and (19), Eq. (12) takes the form

$$\mathbf{F}^C = \nabla[k_B T \ln(1 - b\rho) + a\rho] + \kappa \nabla \nabla^2 \rho. \tag{20}$$

We see from this equation that the conservative force depends on density as well as its gradients. To compute the surface tension term in Eq. (19), we use the definition of density in Eq. (17). We can see from Eq. (19) that the quadratic weight function used in Eq. (7) for dissipative and random forces will not be appropriate for density calculations as we need to calculate higher-order density derivatives in this equation. Hence, the Lucy weight function [52] in Eq. (18) is chosen.

Using the methodology presented above, the interparticle conservative force $\mathbf{F}_{ij}^C$ takes the final form

$$\mathbf{F}_{ij}^C = \left[\underbrace{-\left\{ \left(\frac{bk_B T}{1 - b\rho_i} - a \right) + \left(\frac{bk_B T}{1 - b\rho_j} - a \right) \right\} w_{ij}^{(1)}}_{(a)} + \underbrace{\kappa w_{ij}^{(3)}}_{(b)} \right] \mathbf{e}_{ij}, \tag{21}$$

where $w_{ij}^{(1)}$ and $w_{ij}^{(3)}$ denote the first and third derivatives of the weight function in Eq. (18) with respect to the interparticle separation. In this equation, the term labeled (a) is responsible for phase segregation while the term labeled (b) is responsible for surface tension. So the dissipative and random forces from Eq. (2) and the conservative force from Eq. (21) give the interparticle forces of interaction for the two-phase DPD model. The model for the interparticle conservative force is completely specified by Eqs. (17), (18), and (21).

The parameters that are required for specifying the interparticle conservative force are a, b, κ, r_c, and $k_B T$. The appearance of third derivatives of the weight function in term (b) is related to the form of surface tension force in Eq. (19) and the definition of density in terms of weight function as given by Eq. (17). The amplitude of interparticle conservative force in Eq. (21) depends on functions of density and interparticle separation. In this sense, it is similar to the model proposed by Warren [28,30]. The two-phase model that is developed here is based on mean-field theory. The mean-field theory begins to fail in the vicinity of critical point [50] and the model should not be applied to near-critical systems. The correlations present in the system will also make the mean-field expressions for a and κ in Eq. (11) approximate. Next, we will present the results from test cases that were performed using this two-phase model.

III. NUMERICAL SIMULATIONS

In this section, we will describe several simulations that have been carried out to assess the accuracy of the two-phase DPD model. An important consideration that becomes important for methods like DPD is thermal fluctuations at relatively small scales. When our interest lies in the description of interfacial phenomena, the particles at the interface have energies from thermal motion as well as from surface tension forces. The relative importance of the thermal fluctuations can be assessed by considering a ratio of the thermal length scale l_T to a characteristic physical length scale L. The thermal length scale l_T [33] based on the temperature T and surface tension σ_S is defined as follows:

$$l_T = \sqrt{\frac{k_B T}{\sigma_s}}, \tag{22}$$

where k_B is the Boltzmann constant. When performing simulations involving an interface, this length scale corresponds to that of thermally induced surface fluctuations. For a problem with characteristic physical length L we can define a non-dimensional length l^* as follows:

$$l^* = \frac{L}{l_T}. \tag{23}$$

It is important that $l^* \gg 1$ for us be able to distinguish surface tension related dynamics from thermally induced dynamics. Unless stated otherwise, all the parameters in numerical simulations that follow are in DPD units. All the simulations performed in this work are in two dimensions.

A. Liquid layer simulations

In this section, we will describe the simulation of a two-dimensional liquid layer. The surface tension obtained from this simulation is then compared with the values obtained from simulations carried out to assess the accuracy of the model to reproduce Laplace's law and small-amplitude oscillations of liquid cylinders.

For the two-phase model developed in this work, surface tension is related to the parameter κ through the relationship [50,53]

$$\sigma_s = \kappa \int_{-\infty}^{\infty} \left(\frac{\partial \rho}{\partial n} \right)^2 dn, \tag{24}$$

where σ_s is the surface tension, κ is the surface tension parameter for the two-phase model defined by Eq. (11), ρ is the number density, and n is the direction that is normal to the interface. To perform this calculation, we consider a two-dimensional problem in which a planar interface exists between the liquid and vapor phases. The computational set-up for this problem is shown in Fig. 3. The liquid layer lies in the middle of the computational domain. Periodic boundary conditions [34] are applied along the four boundaries of the computational domain. This simulation was carried out with 10 000 particles, all of which were initially arranged in the liquid layer according to a simple cubic arrangement.

The set of parameters for this simulation is given in Table I. When choosing the simulation parameters, we ensure that we satisfy the mean-field limit, i.e., the ratio of cut-off radius to the average interparticle separation should be much greater than one. The amplitudes for dissipative and random forces are chosen to give a low value of viscosity because the surface tension value from this simulation is compared with the surface tension value obtained from oscillations of liquid

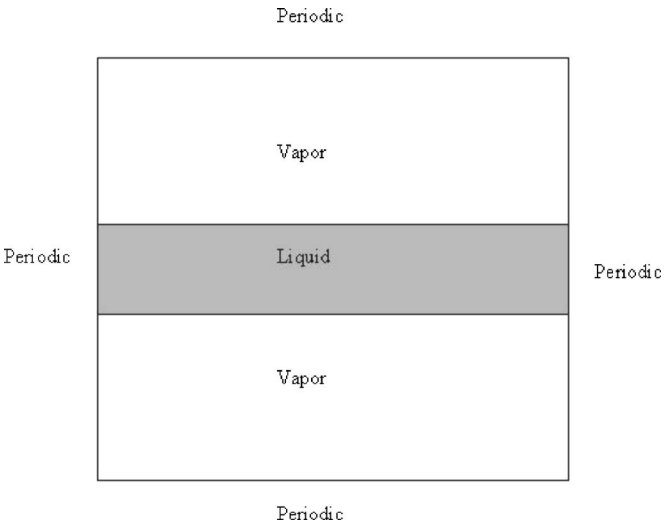

FIG. 3. Computational setup for the liquid layer problem.

cylinders where the analytical solution is available only with an inviscid approximation. The temperature for this simulation is such that $T/T_{\text{critical}}=0.59$. These parameters correspond to a condition in which the ambient is a vacuum. Equation (11) reveals that the value of parameter κ should be smaller than the value of parameter a [49]. We found in our work that the code becomes unstable when κ is increased beyond a certain value. The thickness of the liquid layer being simulated for this problem is about 69 times the thermal length scale defined in Eq. (22).

To analyze the data generated and to get the density profile, we use a post-processing scheme that divides the liquid layer into a number of fine layers of equal thickness. The density inside each fine layer is calculated by counting the number of particles that lie within it and dividing by its volume. For the particular simulation presented here the density profile is obtained by averaging over 800 snapshots of the liquid layer after equilibrium is reached. This is necessary to remove the noise from the data.

TABLE I. Parameters for the simulation of a liquid layer.

Parameter	Equation in which the parameter appears	Value in DPD units
k_BT	(5) and (21)	2.1×10^{-2}
a (van der Waals parameter)	(21)	3.012×10^{-3}
b (van der Waals parameter)	(21)	2.5×10^{-2}
Mean-field critical density	—	13.33
Mean-field critical temperature	—	3.57×10^{-2}
σ	(2)	6.13×10^{-2}
κ	(20)	8.0×10^{-4}
Time step δt	(6) and (8)	1.0×10^{-2}
r_c	(7) and (18)	1.11
N	—	10 000
Domain dimensions ($x\times y$)	—	33.806×33.806

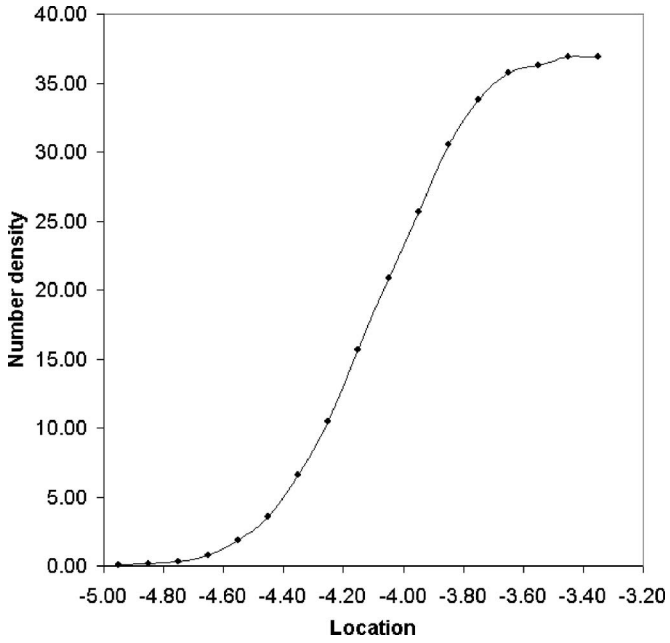

FIG. 4. Interfacial density profile for the liquid layer problem; black dots indicate the average value in a fine layer while the solid line is a fit to this data. Values are in DPD units.

After applying this scheme and splitting the interfacial region into 17 fine layers, we get the interfacial density profile shown in Fig. 4. We see that the density varies smoothly from a high value in the liquid layer to a zero value corresponding to the vacuum surrounding the liquid. This profile is then used to calculate the surface tension from Eq. (24). For performing the numerical integration required in this equation, we use the second-order trapezoidal rule. The surface tension from these calculations is determined to be $\sigma_s=1.15\pm0.01$. The error estimate reported here is determined by using the standard deviation in the mean values of densities in the fine layers. The thickness of the interfacial region was found to be of the same order as the cut-off radius of the DPD model.

B. Laplace law simulations

In this section, we will describe the simulations carried out to assess the ability of the two-phase model to reproduce the Laplace law. This is a standard test case for verification of two-phase models under static conditions. The Laplace law gives a relationship between the pressures inside and outside of a drop at equilibrium. Due to the surface tension effects, the pressure inside a drop is higher than the pressure outside and this pressure differential also depends on the curvature of the drop. The relationship is given by [50]

$$p_{in}-p_{out}=\frac{(d-1)\sigma_s}{R}, \tag{25}$$

where p denotes the pressure, the subscripts *in* and *out* denote the region inside and outside of the drop, respectively, σ_s is the surface tension, R the radius of curvature, and d the dimensionality of the problem.

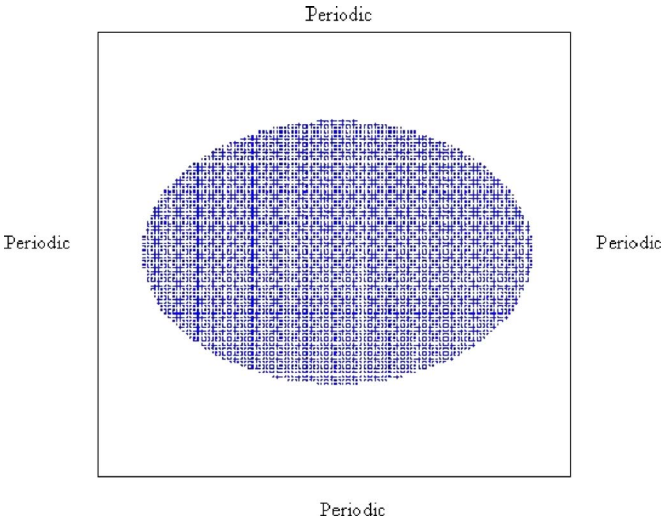

FIG. 5. (Color online) Initial configuration of DPD particles for the Laplace law simulation.

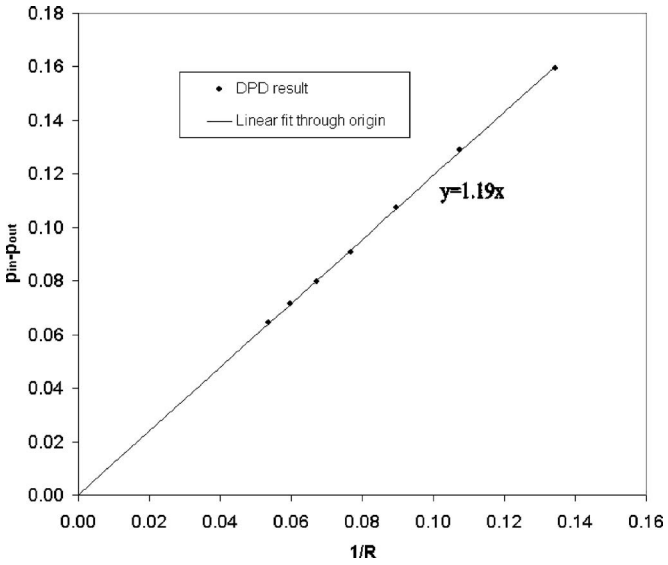

FIG. 6. Verification of Laplace law for the two-phase DPD model. Values are in DPD units.

The simulation parameters are the same as those in Table I. We use the virial equation of state to calculate the pressure of the DPD fluid. The calculation of pressure inside any volume V containing a set of DPD particles can be performed by using the expression [34,54]

$$p = \rho k_B T + \frac{1}{2dV} \sum_i \sum_j \mathbf{r}_{ij} \cdot \mathbf{F}_{ij}^C, \tag{26}$$

where p denotes the pressure, ρ the number density, k_B the Boltzmann constant, T the temperature, d the dimensionality of the problem, V the volume, $\mathbf{r}_{ij}$ the interparticle separation vector, i and j the particle tags, and $\mathbf{F}_{ij}^C$ the conservative part of the DPD interparticle forces. It should be noted that the summation in Eq. (26) should be performed over all particles i that lie *within the volume V* and *all possible particles j that can interact with i* [55]. This definition of pressure is generic and can be used at any point where the pressure is desired. The computations for this test problem were performed in two dimensions and hence the Laplace law for this case is

$$p_{in} - p_{out} = \frac{\sigma_s}{R}. \tag{27}$$

The initial setup for the simulations is shown in Fig. 5. All the particles are arranged inside an elliptical region according to a simple cubic arrangement. The density is set to be equal to the equilibrium value determined from liquid layer simulations. Periodic boundary conditions [34] are applied at the boundaries of the computational domain. The initial shape of the group of particles can be any *regular* arrangement such as triangle, square, or ellipse. By *regular* we mean an arrangement where the initial density is uniform. If such an arrangement is not chosen, the simulations tend to be unstable. All the regular arrangements are equivalent for this simulation because we are interested in the static pressure inside and outside of the drop. After equilibrium is reached, the system has no memory of the initial configuration and it attains a circular shape. The reason for choosing an elliptical configuration is that we use the same computations for oscillation studies of liquid cylinders.

Based on the discussion that we have had so far, we are in a position to calculate pressure inside the liquid cylinder. As pointed out earlier, the simulation parameters that are chosen in this case are such that the vapor phase is of negligible density, which means that essentially we have a vacuum outside the liquid cylinder. To calculate the pressure inside the liquid cylinder, we have chosen a virial radius r that is 0.7 times the equilibrium radius R of the cylinder. This choice has been made to avoid the pressure fluctuations near the interface that may lead to inaccuracies in calculating the pressure inside the drop. To obtain R we use the number density inside the equilibrated cylinder. Using the definition of number density we can get R from the following relationship:

$$R = \sqrt{\frac{N}{\pi \rho_{eq}}}, \tag{28}$$

where N is the number of particles inside the cylinder, and ρ_{eq} is the number density inside the equilibrated cylinder.

We are now in a position to determine the surface tension from Eq. (27). To do this and to establish the relationship between the pressure difference and $1/R$ we performed seven simulations with 6400, 10 000, 14 400, 19 600, 25 600, 32 400, and 40 000 particles, respectively, keeping all other simulation parameters constant. The change in the number of particles results in cylinders of different sizes. The size of the computational domain in DPD units is fixed at 80×80 for all the simulations. The results obtained are presented in Fig. 6. The pressure is calculated by averaging the instantaneous values obtained from Eq. (26) over 50 000 time steps. We see that the pressure difference varies linearly with $1/R$. The data obtained is fitted to a line passing through the origin, and the surface tension σ_s is determined to be 1.19 ± 0.02 in DPD units from Eq. (27). The error estimate reported here is

determined by the standard deviation in the mean value of pressure. It was seen that the pressure inside the liquid cylinder oscillates initially before reaching a steady value because of the non-equilibrium initial condition.

C. Oscillations of a liquid cylinder

Next, we will describe simulations of liquid cylinder oscillations performed to test the two-phase DPD model. This test problem involves simulations under dynamical conditions and is, hence, different in nature from the previous two simulations. We will present the simulation results for cylinders undergoing small-amplitude oscillations and then for cylinders undergoing large-amplitude oscillations. In the case of small-amplitude oscillations, the computed time period will be used for getting the surface tension and this value will be compared with the value obtained from Laplace's law simulations. The setup is the same as that for reproducing Laplace law in the previous section, except that here we are interested in the transient behavior of the cylinder as opposed to the static behavior in the previous case. The liquid cylinder oscillates because the equilibrium shape which minimizes the surface energy is circular. But if we start with a noncircular shape there is a pressure imbalance between points with different local values of radius of curvature. It is this imbalance that makes the cylinders (or drops in three dimensions) oscillate and relax to an equilibrium circular shape.

1. Small-amplitude oscillations

For cylinders undergoing small-amplitude oscillations, the time period T of oscillations has been analytically derived by Rayleigh [56] for an inviscid fluid and is given by

$$T = 2\pi\sqrt{\frac{\rho R^3}{6\sigma_s}}, \tag{29}$$

where ρ denotes the number density, R the equilibrium radius of the circular cylinder, and σ_s the surface tension. A nondimensional Reynolds number Re [57] can be defined in this problem as

$$\mathrm{Re} = \frac{1}{\upsilon}\sqrt{\frac{\sigma_s R}{\rho}}, \tag{30}$$

where υ is the viscosity of the DPD fluid. The time period given by Eq. (29) is valid for the case when $\mathrm{Re} \gg 1$. In the simulations performed here, the Reynolds number is typically of the order of 10 and hence this condition is approximately satisfied. The time period of oscillations obtained from DPD simulations can be used in Eq. (29) to get the value of surface tension, knowing ρ and R.

The computational set-up is shown in Fig. 5. The simulation parameters are the same as those for Laplace law simulations. 10 000 particles are used for this simulation. We start with an elliptical liquid cylinder that has an aspect ratio of 1.4. The particles are placed according to a simple cubic arrangement inside this cylinder. This ellipse is then allowed to evolve with time, and the oscillatory behavior is studied. The transient movement of the interface along the x and y directions is examined. To do this, an averaging procedure in which the coordinates of all the particles within a cell are used to define the interfacial location is employed. We know that the density varies from a high value in the liquid region, ρ_l, to a low value, ρ_v, in the vapor region. We define the interface to be at location where the density is $(\rho_l+\rho_v)/2$. All the particles that lie in a sampling window of thickness $\pm(\rho_l+\rho_v)/8$ on either side of the interface are used for obtaining the interfacial location. The size of the sampling window is selected such that results are size-independent. The diameter of the liquid cylinder being simulated in this problem is 75.6 times the thermal length scale defined in Eq. (22).

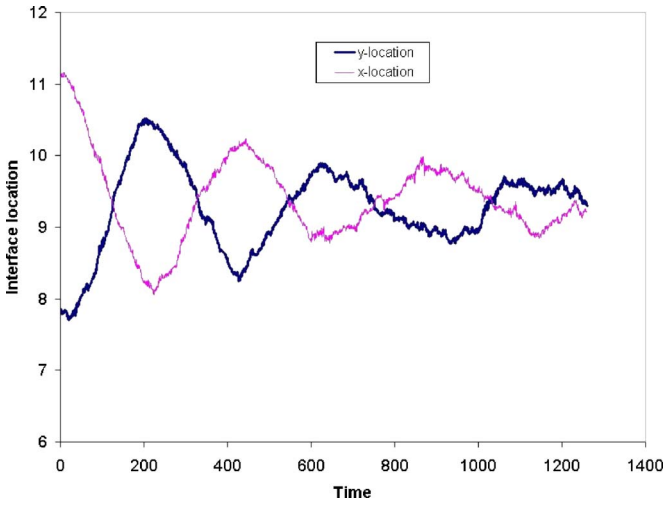

FIG. 7. (Color online) Interfacial location along the x and y axes as a function of time. Values are in DPD units.

Figure 7 shows a plot of the interfacial location along the x and y axes as a function of time. We see that the amplitude of oscillations decays with time. Figure 8 shows snapshots of oscillations of this liquid cylinder. We see that the oscillations have a time period of about 400 time units. Hence, the cylinder changes its orientation by 90° after every 200 time steps. Capillary waves induced by thermal fluctuations are visible on the surface of the liquid cylinder. Such thermally induced capillary waves have also been observed in molecular dynamics simulations done by Arcidiacono *et al.* [57]. Thermal fluctuations are responsible for the fluctuations in interfacial location observed in Fig. 7.

The time period of oscillations from this simulation is 415 ± 10 in DPD units. The value of surface tension, σ_s, estimated by employing Eq. (29) is 1.14 ± 0.06. To determine the error estimate, a fast Fourier transform of the signal in Fig. 7 is performed. The error is determined as the difference between the frequency corresponding to the most powerful signal and weighted-average frequency of other powerful signals. The mean value of σ_s differs from the mean value obtained from the Laplace law simulations by 4.2%. It should be pointed that the analytical solution is for an inviscid case. But, in the DPD method we cannot perform simulations of an inviscid fluid as the dissipative, random and conservative forces always give rise to a viscous fluid.

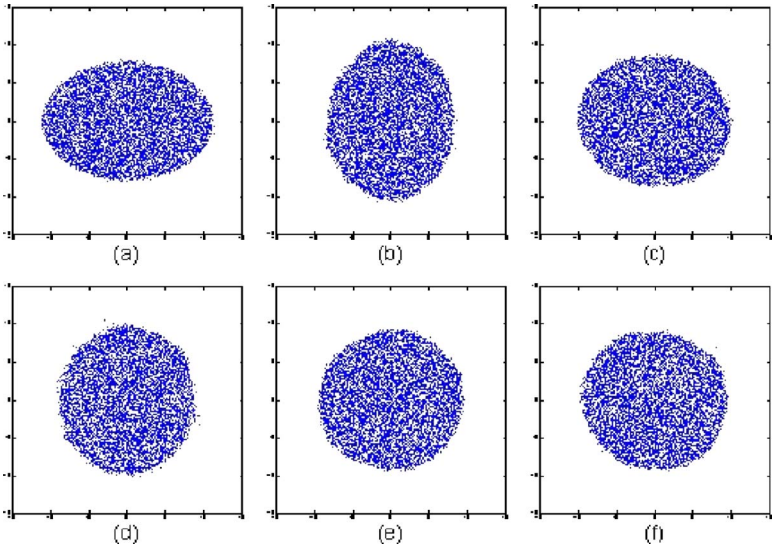

FIG. 8. (Color online) Snapshots of oscillating small-amplitude cylinders at DPD times of (a) 1, (b) 200, (c) 400, (d) 600, (e) 800, and (f) 1000.

2. Large-amplitude oscillations

In this section, we will present the results for large-amplitude oscillations of liquid cylinders. The computational set-up for these simulations is the same as that for small-amplitude oscillations. The initial configuration consists of a liquid cylinder at a density equal to the equilibrium density of the liquid phase. The particles are placed according to a simple cubic arrangement. The difference with the small-amplitude case is that the initial aspect ratio for this case is 5, whereas the aspect ratio for the earlier case was 1.4. In the process of attaining an equilibrium shape, the cylinder undergoes oscillations. Figure 9 shows the results that were obtained in this simulation. We start with the shape shown in Fig. 9(a). The cylinder begins to relax back towards a circular shape. The central part of the cylinder undergoes thinning as seen in Figs. 9(c) and 9(d). It then starts deforming again as seen in Fig. 9(f) because of inertial effects. A thinning of the central part is seen [see Figs. 9(h) and 9(i)]. These shapes for liquids undergoing large amplitude oscillations have been observed experimentally by Apfel *et al.* [58]. Nugent *et al.* [59] have reported similar results using smoothed particle applied mechanics (SPAM).

D. Capillary waves

In this section, we will describe results obtained for capillary wave simulations. These simulations provide an opportunity for testing the two-phase model for a dynamic problem when no-slip boundary conditions are employed on two boundaries.

The analytical expressions for time period and decay rate for this problem are given by Chandrashekar [60]. The time period and oscillation frequency nondimensionalized by $k^{3/2}\sqrt{\sigma_s/(\rho_l+\rho_v)}$ [61] are obtained as real and imaginary parts of

$$n = \frac{y^2 - 1}{\sqrt{s}}, \tag{31}$$

where y is a solution of the quartic equation

$$y^4 + 4\alpha_1\alpha_2 y^3 + 2(1 - 6\alpha_1\alpha_2)y^2 - 4(1 - 3\alpha_1\alpha_2)y + (1 - 4\alpha_1\alpha_2) + s = 0. \tag{32}$$

In the above equations, k denotes the wave number of initial perturbation, σ_s denotes the surface tension, and ρ_l and ρ_v denote the density of liquid and vapor phases, respectively. The quantities s, α_1, and α_2 are defined are follows:

$$s = \frac{\sigma_s}{k(\rho_l + \rho_v)v^2},$$

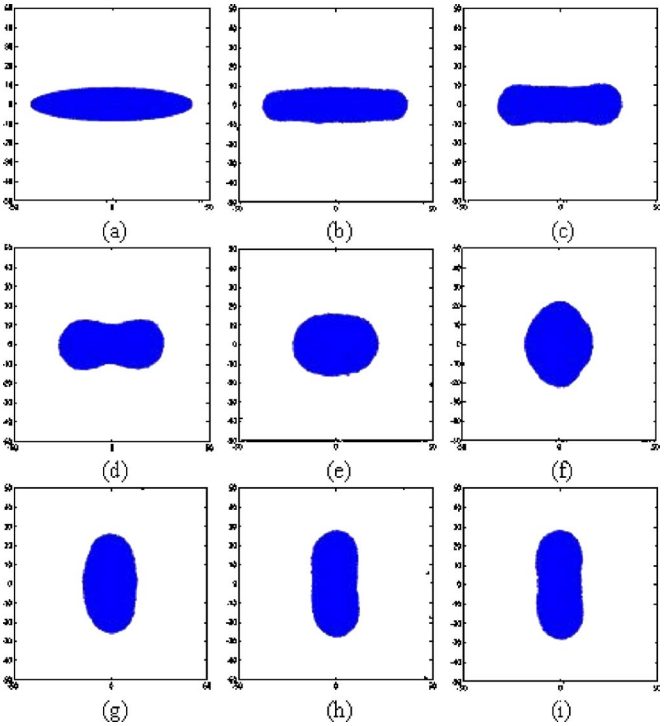

FIG. 9. (Color online) Snapshots of large-amplitude oscillations at DPD times of (a) $t=1$, (b) $t=100$, (c) $t=200$, (d) $t=300$, (e) $t=400$, (f) $t=500$, (g) $t=600$, (h) $t=700$, and (i) $t=800$.

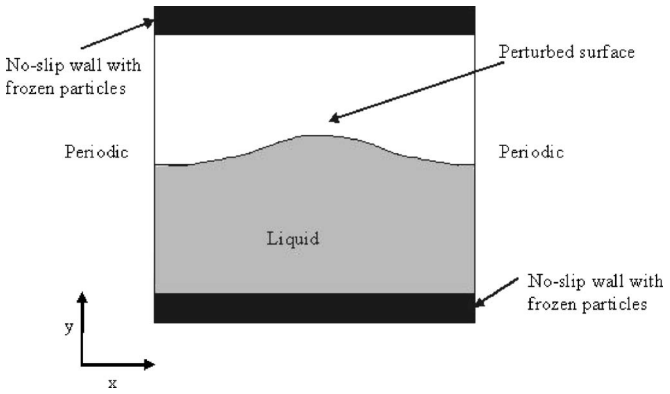

FIG. 10. Computational domain for the simulation of capillary waves.

$$\alpha_1 = \frac{\rho_l}{\rho_l + \rho_v}, \tag{33}$$

and

$$\alpha_2 = \frac{\rho_v}{\rho_l + \rho_v}.$$

The computational setup for this problem is shown in Fig. 10. Periodic boundary conditions [34] are applied along the left and right boundaries and no-slip boundary conditions are used for the top and bottom boundaries.

For implementing the no-slip boundary condition, we use a layer of frozen particles. The particles that try to penetrate this frozen layer are reintroduced into the computational domain by using a bounce-back reflection rule [62]. The density of particles in this frozen layer is taken to be equal to the density of the fluid. It is important to have a correct implementation of this boundary condition as the forces of interaction between DPD particles in the two-phase model are density dependent and erroneous calculation of density near the walls may lead to instabilities in the code. The simulation parameters are the same as those shown in Table I. The dimension of the computational domain was 49.32×49.32 in DPD units. The thicknesses of the top and bottom walls are

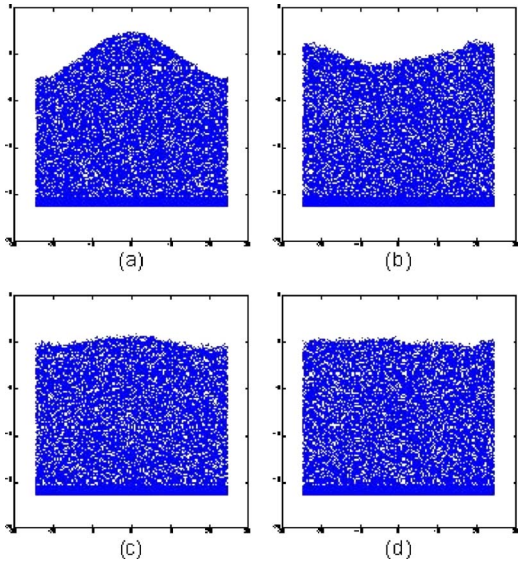

FIG. 11. (Color online) Snapshots of capillary waves at DPD times of (a) 1, (b) 350, (c) 700, and (d) 1000.

equal to the cut-off radius r_c used in Eqs. (7) and (18) for the model. The dimension of the computational domain along the x direction is 372.8 times the thermal length scale defined in Eq. (22). The initial amplitude of the sinusoidal disturbance is 5% of the length of the computational domain along the x direction. The simulation parameters used here correspond to a negligibly small density for the vapor phase. The initial configuration consists of a regular arrangement of particles with a density that corresponds to the equilibrium density in the liquid phase. This simulation was performed using 30 000 particles. Figure 11 shows the snapshots of capillary waves at DPD times of 1, 350, 700, and 1000 units from the start of simulation. We see that the configuration at time of 350 units is inverted compared to the initial configuration. The wave again reverts back close to its initial configuration at a time of 700 units but with reduced amplitude. The oscillations have died down in the final snapshot at time of 1000 units.

Figure 12 shows the oscillations of capillary waves as a

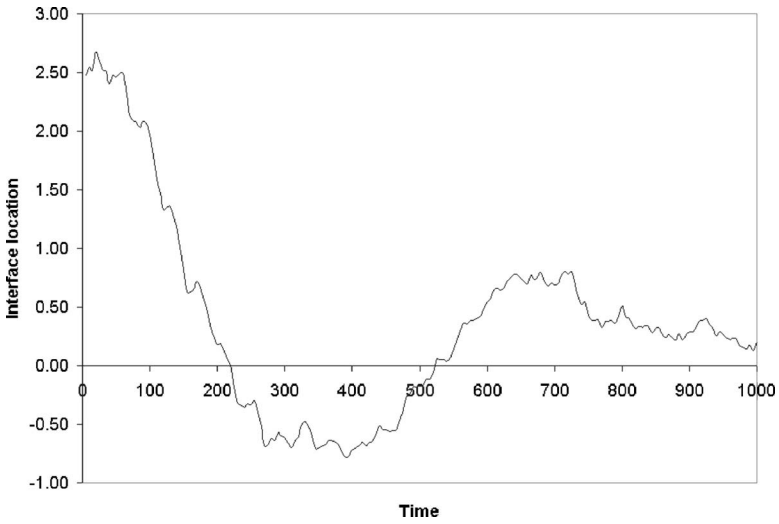

FIG. 12. Location of interface as a function of time. Values are in DPD units.

TABLE II. Parameters used for simulations at low density ratios.

Parameter	Equation in which the parameter appears	Value in DPD units
k_BT	(5) and (21)	0.5, 0.6, 0.7, 0.8, 0.9, and 1.0
a (van der Waals parameter)	(21)	1.0×10^{-1}
b (van der Waals parameter)	(21)	2.5×10^{-2}
Mean-field critical density	—	13.33
Mean-field critical temperature	—	1.19
σ	(2)	2.0
κ	(21)	5.0×10^{-3}
Time step δt	(6) and (8)	1.0×10^{-2}
r_c	(7) and (18)	1.11
N	—	10 000
Domain dimensions (x x y)	—	30.0×30.0

function of time for the simulation presented here. The location of the interface is determined by using the same criteria used in oscillation studies of liquid cylinder. We see from Fig. 12 that the oscillations decay with time. At the time of about 1000 units, the amplitude of capillary waves is of the order of the amplitude of thermal fluctuations and they become indistinguishable from each other. The time period of oscillations obtained from this plot is found to be 680 ± 18 in DPD units. The error estimate in time period is determined using the same method as for small-amplitude oscillations. The decay rate of oscillations from these results is found to be $(1.68\pm0.16)\times10^{-3}$. The error estimate in decay rate is determined by taking the thermal length scale into consideration while calculating the interfacial location. The corresponding values for the time period and decay rate obtained from the analytical solution in Eq. (32) are 757.3 and 1.94×10^{-3}, respectively. When solving Eq. (32), we need to know the surface tension and viscosity of the liquid. Surface tension was determined from the Laplace law simulations reported earlier. Viscosity was determined by simulating a case of Poiseuille flow until steady state was attained. The velocity profile was then compared with the analytical parabolic profile to get the viscosity. The Poiseuille flow simulation was also performed by employing the no-slip boundary condition described in this section.

We see that the time period obtained from DPD simulations differs from the analytical value by 10.2%. The mean value of decay rate differs from the analytical value by 13.4%. This may arise from the fact that the analytical solution for capillary waves does not take the bulk viscosity of the fluid into consideration while this bulk viscosity is present in DPD simulations. Such a difference in decay rates for oscillations of a liquid drop has been observed earlier by Arcidiacono *et al.* [57], and they had attributed the large difference between analytical and computed values of damping constant to the absence of bulk viscosity in the derivation of the analytical solution.

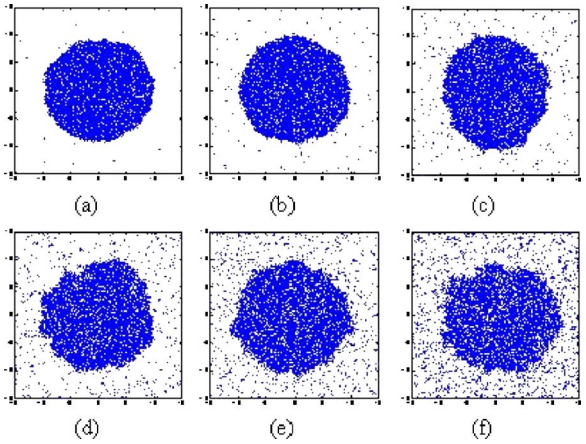

FIG. 13. (Color online) Formation of liquid cylinder at DPD temperatures of (a) 0.5, (b) 0.6, (c) 0.7, (d) 0.8, (e) 0.9, and (f) 1.0. The mean-field critical temperature is 1.19 in DPD units.

E. Simulations at different temperatures

The simulation results that were presented in previous sections were for the case when the ambient is a vacuum. The two-phase model that has been developed in this work, however, is generic and can be used for simulations at lower liquid-to-vapor density ratios. To demonstrate this, we performed simulations at different temperatures. The equilibrium vapor density will be higher at higher temperatures. The simulation parameters are shown in Table II. They correspond to a mean-field critical temperature of 1.19 in DPD units. We performed simulations of liquid cylinder formation starting with a blob of fluid in a two-dimensional periodic box as described in the section on the verification of Laplace law. Figure 13 shows the results at temperatures of 0.5, 0.6, 0.7, 0.8, 0.9, and 1.0. We see that the number of particles in the vapor phase is greater at higher temperatures. This is also

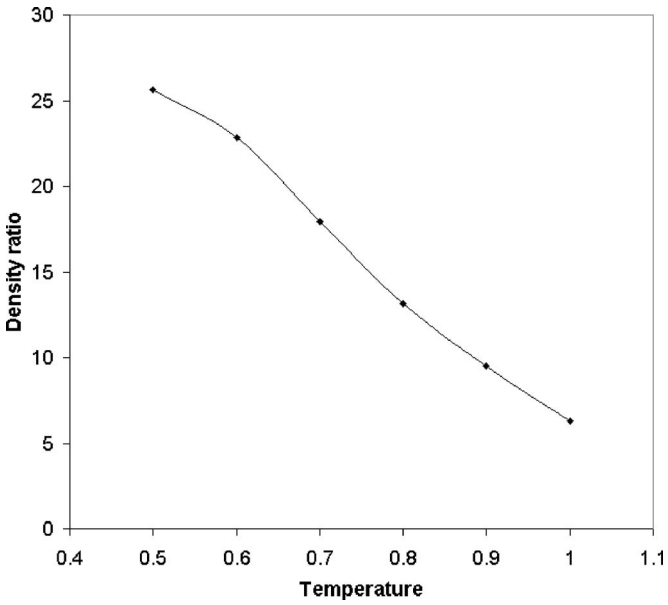

FIG. 14. Equilibrium liquid-to-vapor density ratio at different temperatures. Temperature is in DPD units.

evident in Fig. 14, which shows the computed equilibrium density ratios at different temperatures. We see that the density ratio is lower at higher temperatures.

IV. SUMMARY AND CONCLUSIONS

In this work, we have presented a mean-field theory-based DPD model for two-phase systems involving liquid and vapor phases. In order to have a stable two-phase system, the liquid and vapor phases must be segregated and surface tension should be active in the interfacial region. In the model developed, phase segregation between the two phases arises because of an equation of state with a van der Waals loop. We have used the van der Waals equation of state to provide this feature. Surface tension is modeled by a term that depends on higher-order density gradients and accounts for long-range attractive forces not accounted for in the model. These features enter the DPD system through the conservative force whose amplitude now depends on density and its gradients. The terms dependent on density gradients become important in the interfacial region and give rise to surface tension. The strength of surface tension can be controlled using a free parameter. We have presented several test cases including simulations of a liquid layer, verification of Laplace's law, small- and large-amplitude oscillations of liquid cylinders, and capillary waves. The surface tension obtained from liquid layer simulation differs from that obtained from Laplace law simulations by 3.4%. The surface tension obtained from small-amplitude oscillations of liquid cylinders differs from the Laplace law value by 4.2%. The results from large-amplitude oscillations of liquid cylinders are in qualitative agreement with other published results [58,59]. For capillary wave simulations, the time period, of oscillations differ from the analytical value by about 10%, while a difference of about 14% is observed between the computed and analytical values of decay rate. The difference in decay rate can be attributed to the fact that the analytical solution does not account for bulk viscosity, which is always present in DPD simulations. For simulations involving interfacial dynamics, we have also pointed out the importance of the thermal length scale that accounts for the thermal energy of particles. For such simulations, it is important to have the characteristic dimension of the problem much larger than the thermal length scale. To demonstrate the generic nature of the model in its ability to represent two-phase systems at different density ratios, we also presented results of formation of a liquid cylinder at different temperatures that correspond to different density ratios between the liquid and vapor phases. It is shown that the equilibrium density ratio is lower at higher temperatures, as expected.

[1] G. Tryggvason, B. Bunner, A. Esmaeeli, D. Juric, N. A. Rawahi, W. Tauber, J. Han, S. Nas, and Y. J. Jan, J. Comput. Phys. **169**, 708 (2001).

[2] R. Scardovelli and S. Zaleski, Annu. Rev. Fluid Mech. **31**, 567 (1999).

[3] J. A. Sethian and P. Smereka, Annu. Rev. Fluid Mech. **35**, 341 (2003).

[4] S. Succi, *The Lattice Boltzmann Equation for Fluid Dynamics and Beyond* (Oxford University Press, Oxford, 2001).

[5] S. Chen and G. D. Doolen, Annu. Rev. Fluid Mech. **30**, 329 (1998).

[6] R. R. Nourgaliev, T. N. Dinh, T. G. Theofanous, and D. Joseph, Int. J. Multiphase Flow **29**, 117 (2003).

[7] K. N. Premnath and J. Abraham, Phys. Fluids **17**, 122105 (2005).

[8] M. E. McCracken and J. Abraham, Int. J. Mod. Phys. C **16**, 1671 (2005).

[9] S. Y. Trofimov, E. L. F. Nies, and M. A. J. Michels, J. Chem. Phys. **117**, 9383 (2002).

[10] P. J. Hoogerbrugge and J. M. V. A. Koelman, Europhys. Lett. **19**, 155 (1992).

[11] Y. Kong, C. W. Manke, W. G. Madden, and A. G. Schlijper, J. Chem. Phys. **107**, 592 (1997).

[12] A. G. Schlijper, P. J. Hoogerbrugge, and C. W. Manke, J. Rheol. **39**, 567 (1995).

[13] S. Chen, N. P-. Thien, X. J-. Fan, and B. C. Khoo, J. Non-Newtonian Fluid Mech. **118**, 65 (2004).

[14] V. Symeonidis, G. E. Karniadakis, and B. Caswell, Phys. Rev. Lett. **95**, 076001 (2005).

[15] V. Symeonidis, G. E. Karniadakis, and B. Caswell, Bull. Pol. Acad. Sci.: Tech. Sci. **53**, 395 (2005).

[16] X. Fan, N. P-. Thien, N. T. Yong, X. Wu, and D. Xu, Phys. Fluids **15**, 11 (2003).

[17] Y. Liu, X. Yang, M. Yang, and T. Li, Polymer **45**, 6985 (2004).

[18] E. S. Boek, P. V. Coveney, and H. N. W. Lekkerkerker, J. Phys.: Condens. Matter **8**, 9509 (1996).

[19] E. S. Boek, P. V. Coveney, H. N. W. Lekkerkerker, and P. van der Schoot, Phys. Rev. E **55**, 3124 (1997).

[20] W. Dzwinel, D. A. Yuen, and K. Boryczko, J. Mol. Model. **8**, 33 (2002).

[21] A. T. Clark, M. Lal, J. N. Ruddock, and P. B. Warren, Langmuir **16**, 6342 (2000).

[22] J. L. Jones, M. Lal, J. N. Ruddock, and N. A. Spenley, Faraday Discuss. **112**, 129 (1999).

[23] W. Dzwinel, K. Boryczko, and D. A. Yuen, J. Colloid Interface Sci. **258**, 163 (2003).

[24] P. V. Coveney and K. E. Novik, Phys. Rev. E **54**, 5134 (1996).

[25] W. Dzwinel and D. A. Yuen, Int. J. Mod. Phys. C **12**, 91 (2001).

[26] I. Pagonabarraga and D. Frenkel, Mol. Simul. **25**, 167 (2000).

[27] I. Pagonabarraga and D. Frenkel, J. Chem. Phys. **115**, 5015 (2001).

[28] P. B. Warren, Phys. Rev. E **68**, 066702 (2003).

[29] M. Liu, P. Meakin, and H. Huang, Phys. Fluids **18**, 017101 (2006).

[30] P. B. Warren, Phys. Rev. Lett. **87**, 225702 (2001).

[31] D. M. Anderson, G. B. McFadden, and A. A. Wheeler, Annu. Rev. Fluid Mech. **30**, 139 (1998).

[32] S. Kawano, Phys. Rev. E **58**, 4468 (1998).

[33] M. Moseler and U. Landman, Science **289**, 1165 (2000).

[34] M. P. Allen and D. J. Tildesley, *Computer Simulation of Liquids* (Oxford Science Publications, Oxford, 1987).
[35] D. C. Rapaport, *The Art of Molecular Dynamics Simulations* (Cambridge University Press, Cambridge, 1995).
[36] J. Koplik and J. R. Banavar, Annu. Rev. Fluid Mech. **27**, 257 (1995).
[37] J. B. Avalos and A. D. Mackie, Europhys. Lett. **40**, 141 (1997).
[38] P. Espanol, Europhys. Lett. **40**, 631 (1997).
[39] F. Reif, *Fundamentals of Statistical and Thermal Physics* (McGraw-Hill Book Company, New York, 1965).
[40] R. D. Groot and P. B. Warren, J. Chem. Phys. **107**, 4423 (1997).
[41] R. D. Groot and K. L. Rabone, Biophys. J. **81**, 725 (2001).
[42] T. Soddemann, B. Dunweg, and K. Kremer, Phys. Rev. E **68**, 046702 (2003).
[43] P. Espanol, Phys. Rev. E **52**, 1734 (1995).
[44] C. A. Marsh, G. Backx, and M. H. Ernst, Europhys. Lett. **38**, 411 (1997).
[45] G. T. Evans, J. Chem. Phys. **110**, 1338 (1999).
[46] A. Satoh and T. Majima, J. Colloid Interface Sci. **283**, 251 (2005).
[47] P. Espanol and P. B. Warren, Europhys. Lett. **30**, 191 (1995).
[48] K. Huang, *Statistical Mechanics* (John Wiley & Sons Inc., New York, 1963).
[49] J. D. van der Waals, Verh.-K. Ned. Akad. Wet., Afd. Natuurkd., Eerste Reeks **1**, 56 (1893).
[50] J. S. Rowlinson and B. Widom, *Molecular Theory of Capillarity* (Oxford University Press, Oxford, 1982).
[51] G. R. Liu and M. B. Liu, *Smoothed Particle Hydrodynamics: A Meshfree Particle Method* (World Scientific Publishing Company, Singapore, 2003).
[52] L. B. Lucy, Astronomical J. **82**, 1013 (1977).
[53] H. T. Davis, *Statistical Mechanics of Phases, Interfaces and Thin Films* (VCH Publishers, Inc., New York, 1996).
[54] D. M. Tartakovsky and F. J. Alexander, Comput. Sci. Eng. **7**, 14 (2005).
[55] A. Tartakovsky and P. Meakin, Phys. Rev. E **72**, 026301 (2005).
[56] L. Rayleigh, Proc. R. Soc. London **29**, 71 (1879).
[57] S. Arcidiacono, D. Poulikakos, and Y. Ventikos, Phys. Rev. E **70**, 011505 (2004).
[58] R. E. Apfel, Y. Tian, J. Jankovsky, T. Shi, X. Chen, R. G. Holt, E. Trinh, A. Croonquist, K. C. Thornton, A. Sacco, Jr., C. Coleman, F. W. Leslie, and D. H. Matthiesen, Phys. Rev. Lett. **78**, 1912 (1997).
[59] S. Nugent and H. A. Posch, Phys. Rev. E **62**, 4968 (2000).
[60] S. Chandrasekhar, *Hydrodynamic and Hydromagnetic Stability* (Oxford University Press, Oxford, 1961).
[61] R. Zhang, X. He, and S. Chen, Comput. Phys. Commun. **129**, 121 (2000).
[62] M. Revenga, I. Zuniga, and P. Espanol, Comput. Phys. Commun. **121–122**, 309 (1999).